Title

The MAPK-Alfin-like 7 module negatively regulates ROS scavenging genes to promote NLR-mediated immunity

Journal

Proceedings of the National Academy of Sciences of the United States of America, 120(3)

ISSN

0027-8424

Authors

Zhang, Dingliang

Gao, Zongyu

Zhang, He

et al.

Publication Date

2023-01-17

DOI

10.1073/pnas.2214750120

PNAS RESEARCH ARTICLE | PLANT BIOLOGY

The MAPK-Alfin-like 7 module negatively regulates ROS scavenging genes to promote NLR-mediated immunity

Dingliang Zhang[a], Zongyu Gao[a], He Zhang[a], Yizhou Yang[a], Xinxin Yang[a], Xiaofei Zhao[a], Hailong Guo[b], Ugrappa Nagalakshmi[c], Dawei Li[a], Savithramma P. Dinesh-Kumar[c,1], and Yongliang Zhang[a,1]

Edited by Xinnian Dong, Duke University, Durham, NC; received August 31, 2022; accepted December 12, 2022

Nucleotide-binding leucine-rich repeat (NLR) receptor-mediated immunity includes rapid production of reactive oxygen species (ROS) and transcriptional reprogramming, which is controlled by transcription factors (TFs). Although some TFs have been reported to participate in NLR-mediated immune response, most TFs are transcriptional activators, and whether and how transcriptional repressors regulate NLR-mediated plant defenses remains largely unknown. Here, we show that the Alfin-like 7 (AL7) interacts with N NLR and functions as a transcriptional repressor. Knockdown and knockout of *AL7* compromise *N NLR*-mediated resistance against tobacco mosaic virus, whereas *AL7* overexpression enhances defense, indicating a positive regulatory role for AL7 in immunity. AL7 binds to the promoters of ROS scavenging genes to inhibit their transcription during immune responses. Mitogen-activated protein kinases (MAPKs), salicylic acid-induced protein kinase (SIPK), and wound-induced protein kinase (WIPK) directly interact with and phosphorylate AL7, which impairs the AL7-N interaction and enhances its DNA binding activity, which promotes ROS accumulation and enables immune activation. In addition to N, AL7 is also required for the function of other Toll interleukin 1 receptor/nucleotide-binding/leucine-rich repeats (TNLs) including Roq1 and RRS1-R/RPS4. Our findings reveal a hitherto unknown MAPK-AL7 module that negatively regulates ROS scavenging genes to promote NLR-mediated immunity.

N NLR immune receptor | TMV | Alfin-like 7 | transcriptional repressor | MAPKs

Significance

The transcriptional reprogramming commonly occurs during plant immune responses and is controlled by transcription factors (TFs). However, how transcriptional repressors regulate NLR-mediated plant defenses remains poorly understood. Here, our study reveals that Alfin-like 7 (AL7) is a new transcriptional repressor that directly interacts with the N NLR immune receptor and functions as a positive regulator of immunity. AL7 inhibits the transcription of ROS scavenging genes and acts downstream of MAPK signaling cascade. The DNA binding activity of AL7 is regulated by SIPK/WIPK-mediated phosphorylation. AL7 also functions in other TNLs-mediated cell death. Our findings reveal a new functional module in plant immune signaling and provide insights into the transcriptional regulation of plant immunity.

Plants are frequently threatened by diverse pathogens like fungi, bacteria, nematodes, and viruses due to their sessile lifestyle. During the long-term arms race, plants have evolved a two-layered innate immune system to protect themselves from invading pathogens (1). Plasma membrane localized pattern recognition receptors (PRRs) consisting of receptor-like proteins and receptor-like kinases, which recognize the pathogen-associated molecular patterns such as fungal chitin (2) and bacterial flagellin (3) to initiate the first layer immune responses called pattern-triggered immunity (PTI). Pathogen-encoded effectors or elicitors interfere with different steps in PTI to cause diseases. To overcome this, plants have evolved with nucleotide-binding leucine-rich repeat (NLR) class of receptors that perceive pathogen-encoded effectors or elicitors to induce a second layer of defense named effector-triggered immunity (ETI) (4). These two branches of immune signaling are reported to be mutually dependent to synergistically confer resistance against pathogen infection (5, 6). Although PTI and ETI are discrepant in their origin, they share conserved downstream events like mitogen-activated protein kinase (MAPK) cascade activation, calcium fluxes, reactive oxygen species (ROS) production, and extensive transcriptional reprogramming (7–10), all these downstream events collectively constitute the intricate immune signaling network.

The transcriptional reprogramming in plant immunity controlled by transcription factors (TFs) is critical for accurate activation of both PTI and ETI (10). Intensive studies have been performed to reveal the indispensable role of TFs in resistance pathways especially in ETI. For instance, barley MLA10 NLR interacts with MYB6 to enhance its DNA binding ability and initiate disease resistance signaling (11). Another NLR protein PigmR interacts with the PIBP1 TF and mediates its nuclear localization, thereby conferring full blast resistance (12). Also, the resistance protein CaRGA from chickpea conferred resistance against *Fusarium oxysporum* f. sp. *ciceri* race1 (Foc1), a process that depends on the interaction between CaRGA and WRKY64 TF (13). Although a number of TFs have been reported to participate in NLR-mediated immune response, most of TFs are transcriptional activators, and whether and how transcriptional repressors positively regulate NLR-mediated plant defenses remains largely underexplored.

Over 300 *NLR* genes have been reported to confer resistance against diverse pathogens (14). Among them, *N* gene is one of the first identified *NLR* genes, which contains toll/

Author contributions: D.Z., U.N., D.L., S.P.D.-K., and Y.Z. designed research; D.Z., Z.G., H.Z., X.Y., and Y.Z. performed research; Z.G., Y.Y., H.G., D.L., and Y.Z. contributed new reagents/analytic tools; D.Z., Y.Y., X.Z., U.N., S.P.D.-K., and Y.Z. analyzed data; and D.Z., S.P.D.-K., and Y.Z. wrote the paper.

The authors declare no competing interest.

This article is a PNAS Direct Submission.

[1]To whom correspondence may be addressed. Email: spdineshkumar@ucdavis.edu or cauzhangyl@cau.edu.cn.

This article contains supporting information online at https://www.pnas.org/lookup/suppl/doi:10.1073/pnas.2214750120/-/DCSupplemental.

Published January 9, 2023.

interleukin-1 receptor (TIR) domain at the N terminus that confers resistance to tobacco mosaic virus (TMV) (15). By recognizing 50 kDa helicase domain of TMV (referred to as p50 herein) with N receptor-interacting protein 1 (NRIP1) as the intermediary (16, 17), N dimerizes followed by the activation of MAPK signaling modules (18). Salicylic acid-induced protein kinase (SIPK) and wound-induced protein kinase (WIPK) are two canonical MAPKs that were activated during plant defenses including the *N*-mediated resistance against TMV (19–21). The activated SIPK phosphorylates suppressor of the G2 allele of skp1 (SGT1) to mediate the shift of activated N to the nucleus (22), where it interacts with the TF SQUAMOSA PROMOTER BINDING PROTEIN-like 6 (SPL6) that is essential for *N*-mediated immune response (23). Similarly, three TFs WRKY1, WRKY2, and MYB1 interact with the barley MLA10 NLR and regulate MLA10-mediated plant immunity (11).

We previously identified a number of potential interaction partners of N NLR using TurboID-based proximity labeling (PL) approach (24). Notably, one protein called Alfin-like 7 (AL7) is present in the list with a high score (24). NbAL7 is a member of the Alfin-like (AL) family that had previously been demonstrated to function in plant seed germination and response to abiotic stresses like salt or drought (25–28). However, there is no report on whether NbAL7 functions during biotic stresses. Here, we further confirm the interaction between NbAL7 and N protein and provide a mechanistic function for NbAL7 in immunity. We demonstrate that NbAL7 is a transcriptional repressor, which positively regulates *N*-mediated resistance against TMV by inhibiting the expression of ROS scavenging genes. NbAL7 functions downstream of MAPK signaling cascades and its DNA binding activity is regulated by SIPK/WIPK-mediated phosphorylation. Our study reveals a new functional module involved in the NLR receptor-mediated immunity.

Results

N Interacts with NbAL7 In Vivo and In Vitro. By using TurboID-based PL, we previously identified an AL protein (https://solgenomics.net, Niben101Scf03528g01003.1) as a potential new component of the N NLR immune receptor complex. *Nicotiana benthamiana* AL protein is phylogenetically closely related to *Arabidopsis thaliana* Alfin-like protein 7 (AtAL7) (*SI Appendix*, Fig. S1). Hence, we designated the protein as NbAL7 herein.

To validate the interaction between NbAL7 and N protein identified from TurboID-based PL, we performed bimolecular fluorescence complementation (BiFC) assay. We coexpressed NbAL7 fused to the C terminus of yellow fluorescent protein (YFP) (NbAL7-YFPc) and previously described N fused to the N terminus of YFP (N-YFPn) in the genomic sequence context including its 5′ and 3′ regulatory regions and introns (referred to as gN) (16). BiFC assay showed that NbAL7 interacts with full-length N and the TIR domain of N in the nucleus but not with nuclear-localized RH20 protein control (Fig. 1 *A* and *B*). We also tested the interaction between NbAL7 and the TIR domain of N by using the split luciferase system (29). Coexpression of NbAL7-cLuc and nLuc-TIR in *N. benthamiana* produced strong luminescence, whereas a very weak signal was detected for the control combinations NbAL7-cLuc/nLuc or cLuc/nLuc-TIR (Fig. 1*C*). All proteins in the BiFC and split luciferase assays were successfully expressed as evidenced by immunoblot analysis (*SI Appendix*, Fig. S2 *A*–*C*). To further confirm the interactions, we performed coimmunoprecipitation (Co-IP) assays. MYC-tagged N protein (gN-Myc) (16) and HA-tagged NbAL7 or Citrine were coexpressed in *N. benthamiana*. The results showed that gN-Myc Co-IPs with NbAL7-HA but not with Citrine-HA control (Fig. 1*D*). Similarly, the TIR domain of N also Co-IPs with NbAL7 (Fig. 1*E*). To further examine whether NbAL7 physically interacts with N, we purified glutathione S-transferase (GST)-fused TIR domain and

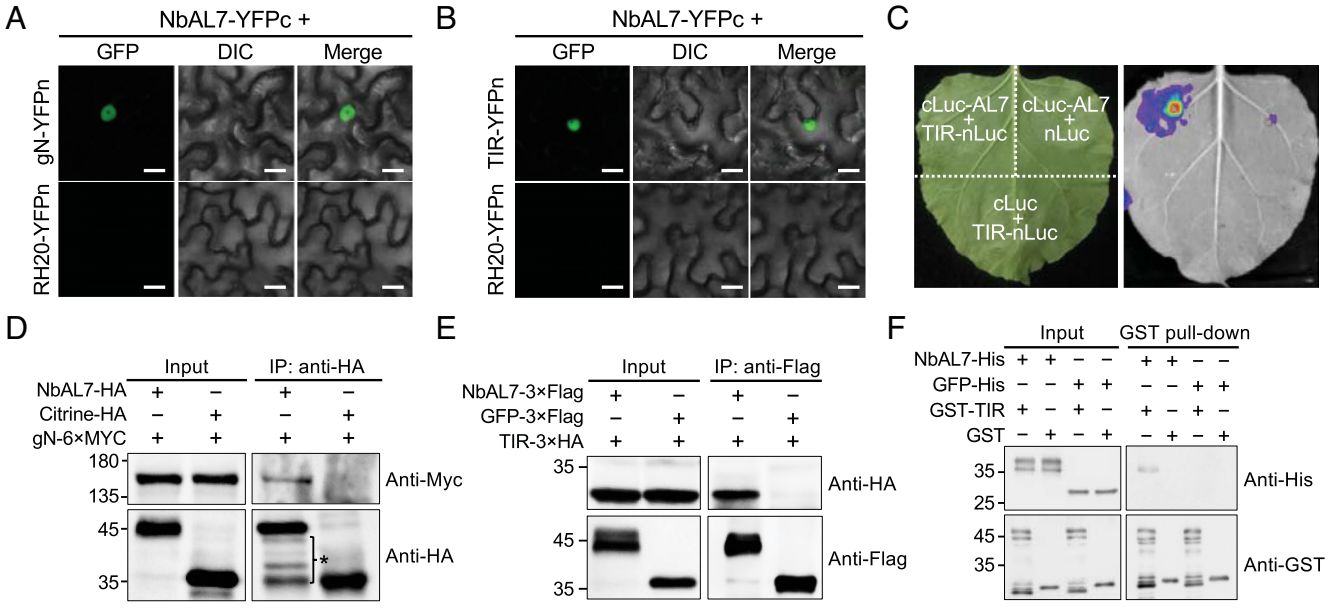

Fig. 1. NbAL7 interacts with N NLR in vivo and in vitro. (*A* and *B*) BiFC to detect the interaction of NbAL7 with N or TIR domain. NbAL7-YFPc was coexpressed with gN-YFPn (*A*) or TIR-YFPn (*B*). NbAL7-YFPc and the RH20-YFPn served as the control. YFP signals were visualized by confocal microscopy at 48 hpi. (Scale bars, 15 μm.) (*C*) Split luciferase assay to detect interaction between NbAL7 and TIR domain. Luminescence signals were recorded in *N. benthamiana* leaves at 48 hpi. (*D* and *E*) Co-IP assay to analyze the interaction of NbAL7 with N (*D*) or TIR domain (*E*). Leaf tissues agroinfiltrated with different combinations indicated above the panels were harvested at 48 hpi. Total proteins were immunoprecipitated with anti-HA (*D*) or anti-Flag beads (*E*). Input and immunoprecipitation (IP) products were analyzed by western blot with anti-HA, anti-Myc, or anti-Flag antibodies. Asterisk in panel *D* indicates protein bands that might be a degradation product of NbAL7-HA. (*F*) GST pull-down analysis of the interaction between NbAL7 and TIR domain. NbAL7-His or GFP-His was incubated with GST-TIR or GST. Input and pull-down products were analyzed by western blot with anti-His and anti-GST antibodies.

NbAL7-His proteins from *Escherichia coli* (Fig. 1*F*); the GST pull-down assay showed that GST-TIR specifically binds to the NbAL7-His protein but not the green fluorescent protein (GFP)-His control. Collectively, these results demonstrate that NbAL7 interacts with N in vivo and in vitro.

NbAL7 Positively Regulates *N TNL*-Mediated Resistance Against TMV. To test whether NbAL7 participates in *N*-mediated immunity, we first evaluated the transcription of *NbAL7* in *N. benthamiana* expressing N (*NN*) (30) after mechanical inoculation with TMV-U1 virions. RT-qPCR analysis revealed that the transcript level of *NbAL7* was elevated at 12 h post TMV infection (hpi) and then decreased at 36 hpi. However, *NbAL7* expression is induced again at 72 hpi. In contrast, the messenger RNA (mRNA) level of *NbAL7* in mock-inoculated *NN* showed no apparent changes (Fig. 2*A*), indicating that NbAL7 may function in *N*-mediated defense against TMV.

Next, we tested the requirement of NbAL7 in *N*-mediated cell death in response to TMV p50. For this, the intron-spliced hairpin RNA-mediated RNA interference was used to downregulate the

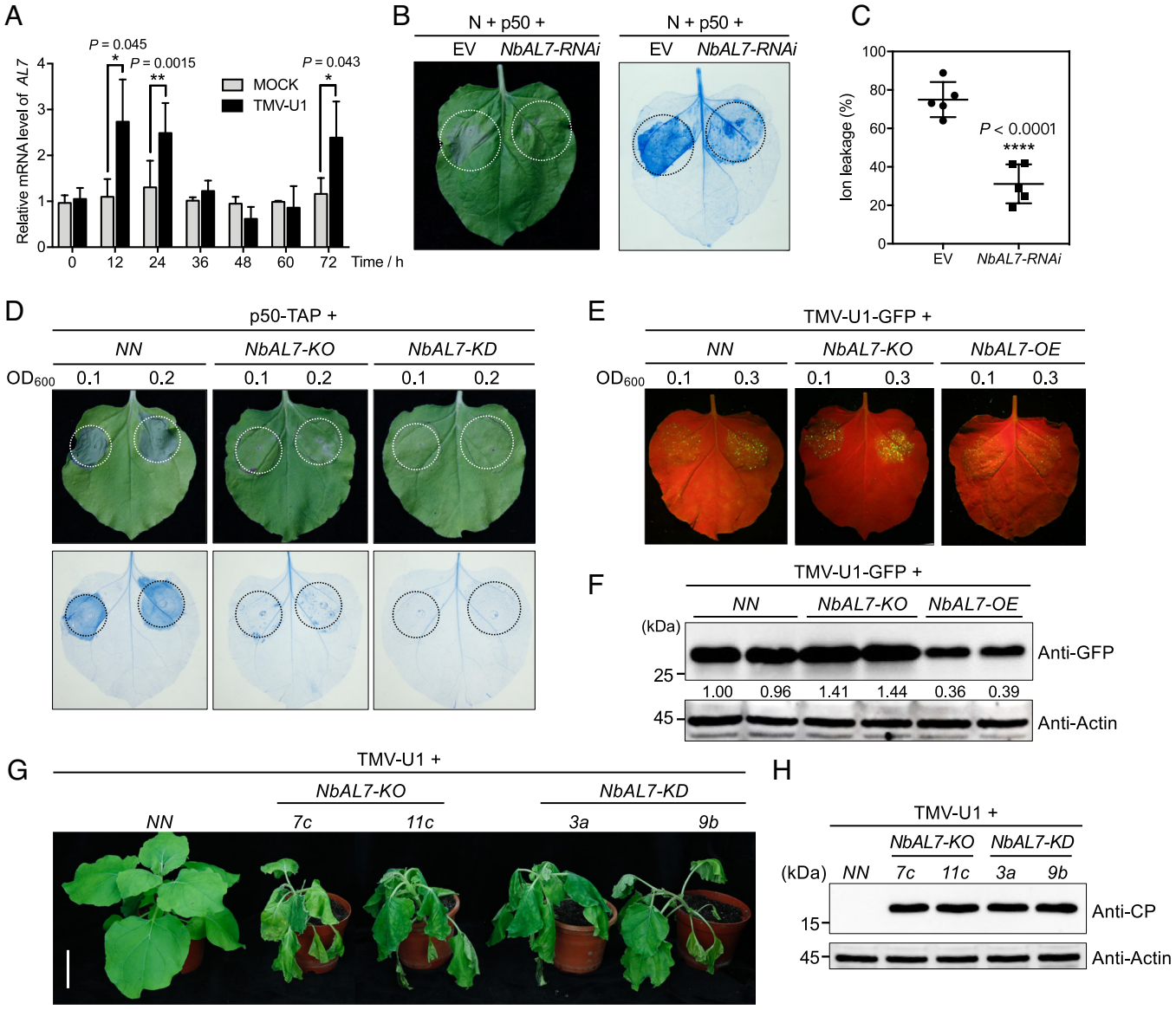

Fig. 2. NbAL7 positively regulates *N*-mediated resistance against TMV. (*A*) The transcript levels of *NbAL7* in *NN* plants during TMV-U1 infection. Total RNA was extracted from the leaves at the indicated time points after mechanical inoculation of TMV-U1 virions. Mock-inoculated (0.01 M phosphate buffered saline) *NN* plants served as the control. (*B*) Knock-down of *NbAL7* impaired p50-induced cell death. Different leaf regions were infiltrated with *Agrobacterium* harboring intron-hairpin NbAL7 or empty vector (EV). After 24 hours, *Agrobacterium* mixtures containing plasmids expressing Myc-tagged N and tandem affinity purification (TAP)-tagged p50 were infiltrated into previously infiltrated regions. Leaves were stained by trypan blue and representative photographs were taken at 4 days post-infiltration (dpi). (*C*) Analysis of ion leakage from the infiltrated leaf regions shown in (*B*). For panels A and C, error bars represent mean ± SD (n = 3 and n = 5 biologically independent plants for panels A and C, respectively). Asterisks indicated significant differences based on two-sided paired Student's *t*-test (*$P < 0.05$, **$P < 0.01$, ****$P < 0.0001$). (*D*) p50-induced cell death was impaired in *NbAL7-KO* and *-KD* transgenic plants. p50-TAP was transiently expressed in the leaves of *NN*, *NbAL7-KO* or *NbAL7-KD* plants. At 4 dpi, the infiltrated leaves were stained by trypan blue and representative photographs were taken. The experiments were repeated three times with similar results. (*E*) *N*-mediated resistance against TMV was compromised by knock-out of *NbAL7* but enhanced by overexpression of *NbAL7*. TMV-U1-GFP at final OD_{600} of 0.1 and 0.3 were agroinoculated onto *NN*, *NbAL7-KO*, and *NbAL7-OE* plants. Photographs were taken under ultraviolet light at 5 dpi. (*F*) Western blot analysis with anti-GFP antibody to detect the accumulation of TMV-U1-GFP in (*E*). Actin served as the loading control. (*G*) Phenotypes of TMV-infected *NN*, *NbAL7-KO* and *NbAL7-KD* plants. *N. benthamiana* leaves were inoculated with 300 ng TMV-U1 virions and photographs were taken at 10 dpi. Bar = 5 cm. (*H*) Western blot analysis with anti-coat protein (CP) antibody to detect the TMV accumulation in the systemic leaves of the plants shown in (*G*). Actin served as the loading control. For panels *E* to *H*, the experiments were independently repeated twice with similar results.

expression of *NbAL7*. The downregulation of the *NbAL7* mRNA level was confirmed by RT-qPCR (*SI Appendix*, Fig. S3*A*). *Agrobacterium* containing RNA interference (RNAi) vector was infiltrated into *N. benthamiana* leaves 24 h prior to infiltration of *Agrobacterium* mixtures expressing gN and p50, whose coexpression activates plant immunity and triggers cell death (17). Trypan blue staining and the ion leakage measurement assay showed that p50-induced cell death was significantly impaired in the regions treated with *NbAL7*-RNAi vector compared with empty vector (EV) (Fig. 2 *B* and *C*). Moreover, GFP-tagged TMV-U1 showed stronger fluorescence in the *NbAL7*-silenced leaf region (*SI Appendix*, Fig. S3 *B*, *Right*) than in the EV control (*SI Appendix*, Fig. S3 *B*, *Left*), and immunoblot analysis showed increased TMV-GFP accumulation in *NbAL7*-silenced leaf region compared with the EV control (*SI Appendix*, Fig. S3*C*).

To further confirm the role of NbAL7 in *N*-mediated defense, we generated *NbAL7* knockout (*NbAL7-KO*), knockdown (*NbAL7-KD*), and overexpression (*NbAL7-OE*) transgenic *NN* plants. Sanger sequencing revealed the deletion of different sizes at the *NbAL7* target site in two *NbAL7-KO* lines (*SI Appendix*, Fig. S4*A*). *NbAL7* mRNA levels were significantly decreased in two independent transgenic lines of *NbAL7-KD* plants compared with *NN* plants, as evidenced by RT-qPCR (*SI Appendix*, Fig. S4*B*). Overexpression of NbAL7 in two independent transgenic lines of *NbAL7-OE* plants was also verified by immunoblot analysis (*SI Appendix*, Fig. S4*C*). The *NbAL7-KO* transgenic plants showed a phenotype of delayed seed germination compared with nontransgenic *NN* plants, while we did not observe obvious differences between *NbAL7-KO* and nontransgenic *NN* plants when they grew up (*SI Appendix*, Fig. S4 *D* and *E*). This is reasonable as previous studies indicated that AtAL7 functions in promoting seed germination (26).

To test the effect on cell death, we infiltrated leaves of *NbAL7-KO* and *NbAL7-KD* transgenic plants with *Agrobacterium* carrying a TAP-tagged p50 at OD_{600} of 0.1 and 0.2. The results showed that the p50 can induce cell death in *NN* plants but it is significantly compromised in either *NbAL7-KO* or *NbAL7-KD* plants (Fig. 2*D*). We then agroinoculated TMV-U1-GFP onto *NN*, *NbAL7-KO*, and *NbAL7-OE* plants. TMV-U1-GFP showed stronger fluorescence in *NbAL7-KO* plants compared with the *NN* plants. In contrast, GFP fluorescence in *NbAL7-OE* plants was weaker than in the control *NN* plants (Fig. 2*E*). Immunoblot analysis further confirmed increased TMV accumulation in *NbAL7-KO* plants and decreased level of TMV in *NbAL7-OE* plants compared with the *NN* plants (Fig. 2*F*). We also rub-inoculated the TMV-U1 virions onto the *NN* or *NbAL7-KO* plants and analyzed the TMV accumulation in the inoculated leaves at 0, 3, 4, and 5 d postinoculation (dpi). Immunoblot analysis showed that the TMV accumulation in the inoculated leaves of *NbAL7-KO* is much higher than that in nontransgenic *NN* plants (*SI Appendix*, Fig. S3*D*). At 10 d after TMV inoculation, both *NbAL7-KO* and *NbAL7-KD N. benthamiana* plants showed obvious wilting phenotype, in striking contrast with the nontransgenic *NN* plants which showed a normal growth (Fig. 2*G*). Immunoblot analysis verified the presence of TMV in upper uninoculated leaves of both *NbAL7-KO* and *NbAL7-KD* plants but not in *NN* plants (Fig. 2*H*). Altogether, these data demonstrated that disruption of *NbAL7* expression significantly compromises *N*-mediated resistance against TMV, indicating the positive regulatory role for NbAL7 in *N*-mediated defense responses.

NbAL7 Is a Transcriptional Repressor and Regulates Defense-Related Genes. To analyze the characteristics of NbAL7, we expressed mCherry-tagged NbAL7 in *N. benthamiana* leaves and observed that NbAL7 localizes to the nucleus (*SI Appendix*, Fig. S5*A*). Furthermore, we performed nuclear isolation assays, and the results showed that NbAL7 was only detected in the nuclear fraction but not in the cytoplasm (*SI Appendix*, Fig. S5*B*). We also used yeast one-hybrid assay to examine its transcriptional activation capability. Results showed that the combination of NbAL7 and the empty pGBKT7 vector did not result in the growth of the yeast on the SD/-Trp-Leu-His-Ade dropout plate, in contrast to that of MYC2 transcription activator (31) (*SI Appendix*, Fig. S5*C*). Dual-luciferase assays showed that the luminescence intensity and ratio of firefly luciferase/Renilla luciferase (LUC/REN) were significantly increased when the positive control VP16 protein was expressed. In contrast, the coexpression of NbAL7 with reporter construct resulted in a significantly decreased luciferase activity compared with EV control (*SI Appendix*, Fig. S5*D*). The expression of the NbAL7 protein was confirmed by immunoblot analysis (*SI Appendix*, Fig. S2*D*). These results indicated that NbAL7 is a nuclear-localized transcriptional repressor.

To identify genes that were targeted by NbAL7, we performed chromatin immunoprecipitation (ChIP)-seq analysis by infiltrating leaves of *N. benthamiana* plants with *Agrobacterium* carrying a hemagglutinin (HA)-tagged NbAL7. The results showed that 2094 genes were enriched (65). Among them, over 75% of the identified peak regions were located in promoter regions upstream of the transcription start site or 5′ intergenic regions, and less than 5% of the peaks were located in exon and intronic regions (Fig. 3*A*). The genome-wide distribution of peak regions analysis showed that that NbAL7 binding site localizes to the transcription start sites of its target genes (Fig. 3*B*). Gene ontology analysis further revealed that specific target genes of NbAL7 were enriched in several biological processes such as intracellular signal transduction, regulation of biological process, signal transduction, and cell communication (Fig. 3*C*).

Given that NbAL7 is a transcriptional repressor that positively regulates *N*-mediated defense, we focused on putative targets that might negatively regulate immune signaling as listed in *SI Appendix*, Table S1. Among them, *L-ascorbate peroxidase 2* (*APX2*), *Glutathione reductase* (*GR*), and *Glutathione peroxidase 2* (*GPX2*) drew our attention. Cytosolic ascorbate peroxidase was reported to respond to ROS production in *Nicotiana tabacum* cv. Xanthi NN plants during TMV infection (32). GR and GPX are also crucial enzymes involved in the ROS scavenging pathway (33–35). The removal of ROS has been widely proved to be an event that is correlated with suppression of plant immunity (36–38). ChIP analysis revealed DNA fragments corresponding to the promoters of these three genes can be enriched by NbAL7 (*SI Appendix*, Fig. S6*A*). By analyzing the promoter sequence of putative *NbAPX2*, *NbGR*, and *NbGPX2*, G-rich elements (GTGGNG or GNGGTG), which have been reported to be targeted by AL family transcriptional regulators (27), were found to be present in the promoters of these three genes (*SI Appendix*, Fig. S6*B*). ChIP-qPCR was conducted to further validate the result of ChIP-seq. The results revealed that NbAL7 was enriched at the G-rich regions of promoters of *NbAPX2*, *NbGR*, and *NbGPX2 in planta*. By contrast, only trace amounts of DNA products were immunoprecipitated when the antibody for enrichment was omitted (Fig. 3*D*). Immunoblot analysis verified the expression of NbAL7 in the *N. benthamiana* leaves as well as the enrichment of NbAL7 in the ChIP assay (*SI Appendix*, Fig. S2*E*).

We carried out competition analysis by electrophoretic mobility shift assay (EMSA) to analyze the direct interaction between NbAL7 and promoters of its target genes. The G-rich element containing regions, including −1,269 to −1,244 bp of *NbAPX2*, −1,289 to −1,264 of *NbGPX2*, and −100 to −73 bp of *NbGR* that were upstream of translation start codon, were designed as

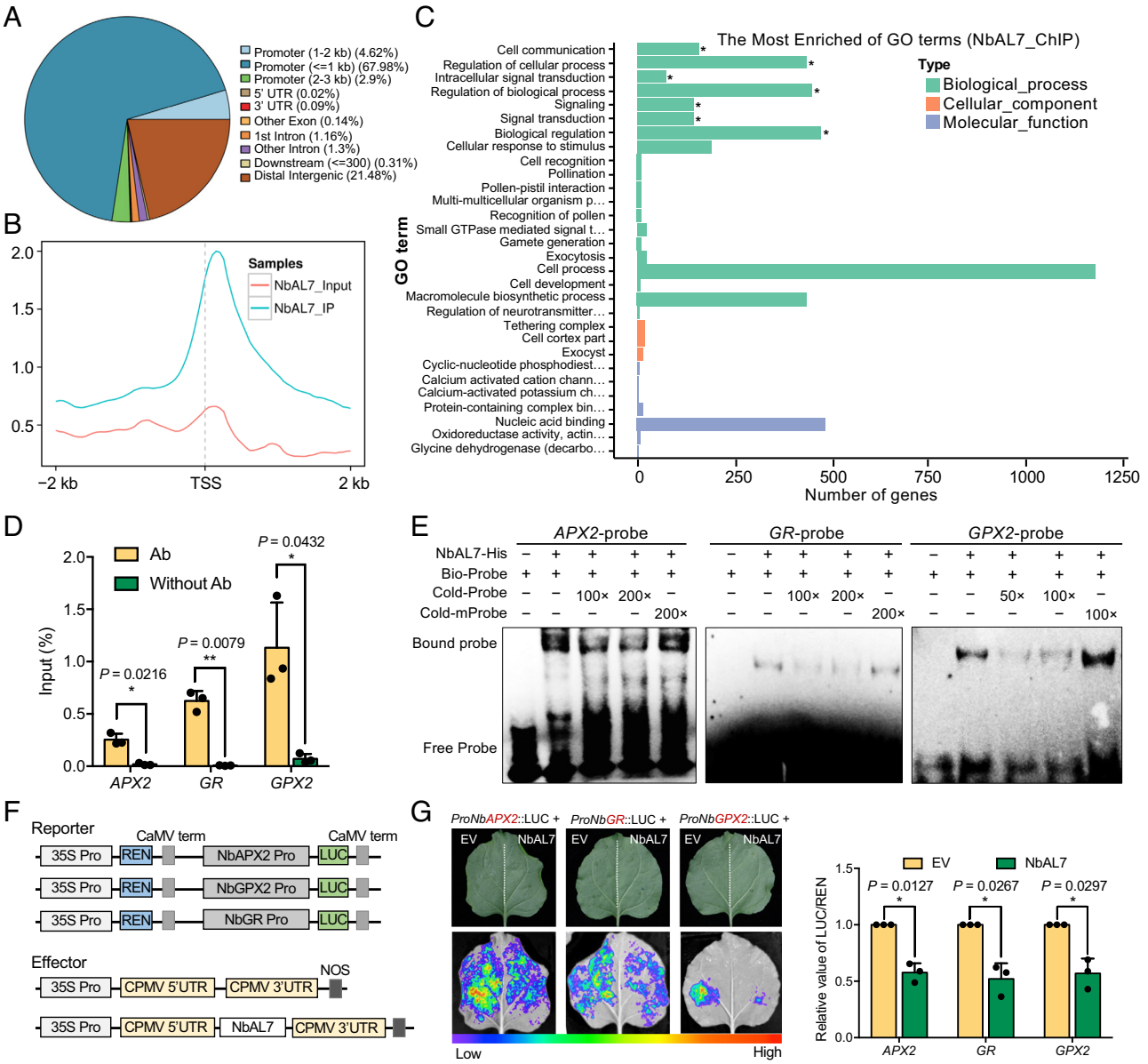

Fig. 3. NbAL7 transcriptionally represses the expression of ROS scavenging genes via directly binding to their promoters. (*A*) Distribution of the NbAL7 binding site location relative to RefSeq genes. Locations of binding sites are divided into promoter (1 to 2 kb), promoter (≤1 kb), promoter (2 to 3 kb), 5′UTR, 3′UTR, other exons, first intron, other introns, and downstream and distal intergenic regions. (*B*) Distribution of identified NbAL7 binding sites relative to the transcriptional start site. (*C*) Analysis of the enriched Gene Ontology (GO) terms. Targeted genes were summarized into three main GO categories: biological process (green box), cellular components (orange red box), and molecular functions (blue box). The x-axis indicates the gene number, and the y-axis indicates the subcategories. Black asterisks indicate significantly enriched terms. The top 30 enriched GO terms were listed. (*D*) ChIP-qPCR assay showing the binding of NbAL7 to the *NbAPX2, NbGR*, and *NbGPX2* promoters in planta. (*E*) EMSA analysis of NbAL7 binding to *NbAPX2, NbGR*, and *NbGPX2* promoters; 26 to 28 bp sequences with G-rich elements of *NbAPX, NbGR*, and *NbGPX2* promoters were designed as probes. (*F*) Dual luciferase reporter system to test the effect of NbAL7 on the transcription of *NbAPX2, NbGR*, and *NbGPX2*. *Upper*: schematic representation of reporter and effector constructs. *Middle*: live imaging of transcriptional repression activity of NbAL7 on promoters of *NbAPX2, NbGR*, and *NbGPX2*. *Bottom*: quantitative analysis of transcriptional repression activity of NbAL7. LUC activity was measured by normalizing to the REN signal. For panels *D* and *G*, error bars indicated mean ± SD (n = 3 biologically independent plants). Asterisks indicated the significant difference based on two-sided paired Student's *t* test (*$P < 0.05$, **$P < 0.01$).

biotin-labeled probes. The same sequence without a biotin label served as the cold probe, and the probes where G-rich elements are substituted with A were used as mutated probes. The results showed that NbAL7 is capable of binding to the biotin-labeled probe, and the unlabeled probe can competitively interfere with the biotin-labeled probe binding to NbAL7 protein, although the *APX2* cold probe did not perform as well as that of *GPX2* and *GR*. In contrast, the unlabeled mutated probe has no obvious effect on the binding between biotin-labeled probe and NbAL7, indicating that NbAL7 specifically binds to G-rich elements within the target genes' promoters (Fig. 3*E*).

To determine the effect of NbAL7 on the target gene expression *in planta*, we performed dual-luciferase assays. Luciferase under the promoters of *NbAPX2*, *NbGR*, and *NbGPX2* was coexpressed with NbAL7 or EV control (Fig. 3*F*). Luminescence intensity and the ratio of LUC/REN served as the indicators of luciferase activity as well as the transcriptional level of *NbAPX2*, *NbGR*, and *NbGPX2*. The results showed that compared with the EV control, NbAL7 expression reduced transcription levels of these three target genes (Fig. 3*G*). The expression of NbAL7 was confirmed by immunoblot (*SI Appendix*, Fig. S2*F*). Moreover, we also analyzed the transcription of *NbAPX2*, *NbGR*, and *NbGPX2* in *NbAL7-KO* transgenic plants;

the results showed that the mRNA levels of these three genes were significantly elevated in *NbAL7-KO* plants compared with *NN* plants (*SI Appendix*, Fig. S6*C*). Together, these results indicate that NbAL7 negatively regulates the transcription of *APX2*, *GR*, and *GPX2* by directly binding to the G-rich element of their promoters.

NbAL7 Contributes to ROS Accumulation and Cell Death. *APX2*, *GR*, and *GPX2* are involved in scavenging of ROS, which plays an important role in both PTI and ETI signaling pathways (39). Overproduction or over accumulation of ROS gives rise to cell death. To verify if NbAL7 participates in the regulation of ROS production and cell death, we transiently overexpressed NbAL7 in *N. benthamiana* leaves, and 3,3′-diaminobenzidine (DAB) staining of the leaves indicated that overexpression of NbAL7 indeed resulted in the increase of ROS accumulation (Fig. 4*A*). Furthermore, H_2O_2 level was measured with Amplex red hydrogen peroxide/peroxidase assay kit, and the results showed that NbAL7 overexpression induced a 3.5-fold higher H_2O_2 level than that of the EV control (Fig. 4*B*). We also observed cell death in the leaves overexpressing NbAL7 as indicated by trypan blue staining, and the ion leakage measurement assay further confirmed it (Fig. 4 *C* and *D*). The expression of NbAL7-HA was verified by immunoblot analysis (*SI Appendix*, Fig. S2*G*).

Given that TMV infection in *NN* plants can induce ROS generation to enhance the immunity against TMV (40, 41), we explored the role of NbAL7 in TMV-induced ROS accumulation in *NN* plants. For this, we analyzed the expression of *NbAPX2*, *NbGR*, and *NbGPX2* in *NN* and *NbAL7-KO* plants upon TMV inoculation. The results showed that their expression was significantly elevated in *NbAL7-KO* plants compared with *NN* plants during TMV infection (Fig. 4*E*). Correspondingly, ROS accumulation in *NbAL7-KO* and *NbAL7-KD* plants infected with TMV at 48 and 72 hpi was much lower than that in *NN* plants as evidenced by DAB staining and H_2O_2 measurement (Fig. 4 *F* and *G*). Together, these results indicate that NbAL7 positively regulates ROS accumulation by repressing the expression of ROS scavenging genes.

SIPK/WIPK Interact with and Phosphorylate NbAL7. Phosphorylation of TFs plays an important role in TF regulation. To investigate whether NbAL7 gets phosphorylated, we purified recombinant NbAL7-His protein from *E. coli*. In an in vitro phosphorylation assay, NbAL7 was phosphorylated by *N. benthamiana* soluble protein extract (Fig. 5*A*).

Previously, using functional protein microarrays, *Arabidopsis* ortholog of NbAL7 has been shown to be phosphorylated by

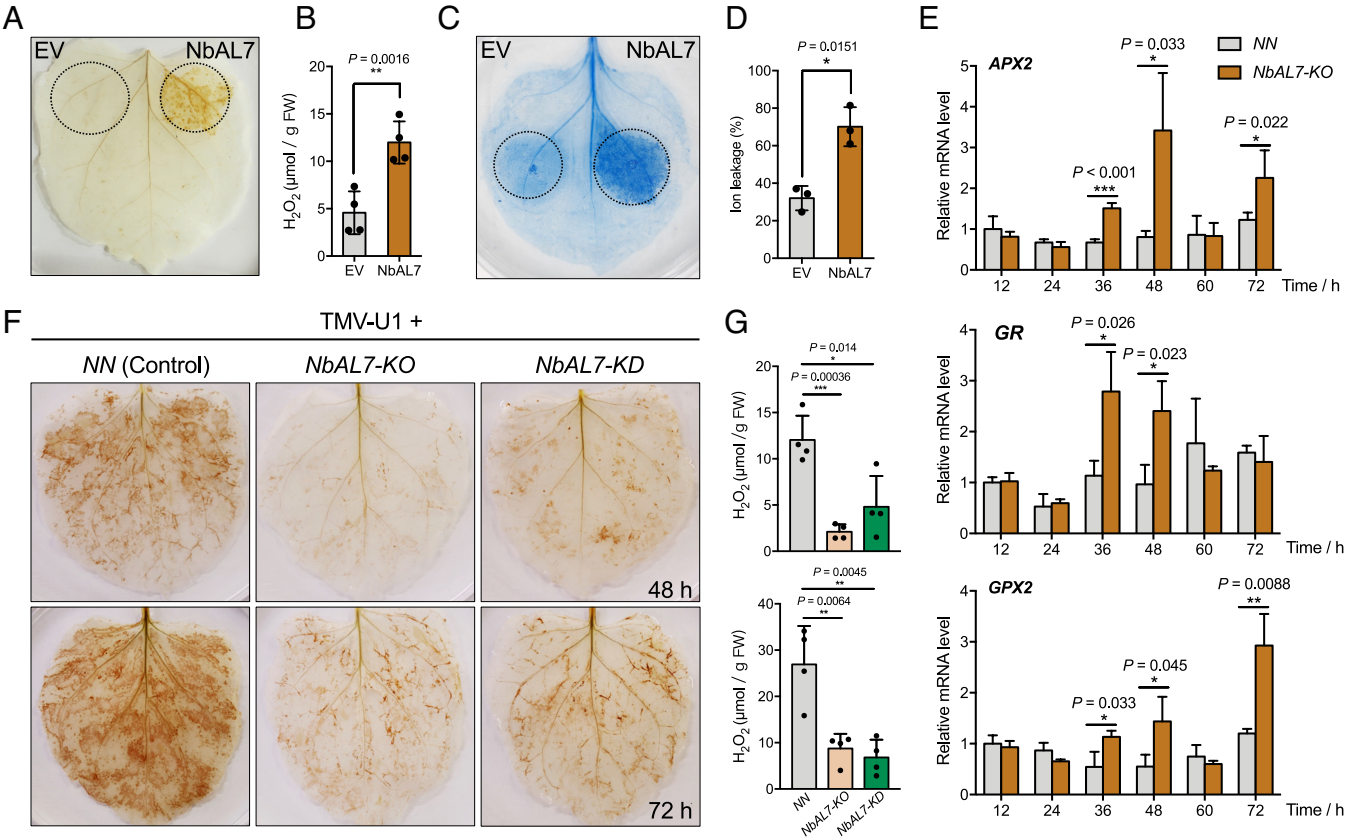

Fig. 4. NbAL7 is required for ROS accumulation in *NN* plants during TMV infection. (*A*) Analysis of NbAL7-induced H_2O_2 accumulation by DAB staining. *Agrobacterium* harboring EV vector or plasmid expressing NbAL7-HA was infiltrated into *N. benthamiana* leaves. At 4 dpi, leaves were stained by DAB and photographs were taken. (*B*) Quantification of H_2O_2 accumulation in *A*. (*C*) Analysis of NbAL7-induced cell death by trypan blue staining. *Agrobacterium* harboring different plasmids was infiltrated into *N. benthamiana* leaves as described in panel *A*. Leaves were stained by trypan blue at 4 dpi, and photographs were taken. (*D*) Analysis of ion leakage from the infiltrated leaf regions shown in *C*. (*E*) The transcript levels of the *APX2, GR*, and *GPX2* gene in *NN* or *NbAL7-KO* plants inoculated with TMV-U1. Total RNA was extracted from the leaves at the indicated time points after inoculation of 300 ng TMV-U1 virions. (*F*) Analysis of ROS accumulation in *NN, NbAL7-KO*, and *NbAL7-KD* plants during TMV infection by DAB staining. Leaves of *NN, NbAL7-KO*, and *NbAL7-KD* plants infected with 300 ng TMV-U1 virions were stained by DAB at 48 hpi (*Upper*) and 72 hpi (*Bottom*). (*G*) Quantification of H_2O_2 accumulation in *F. Upper*: H_2O_2 level in TMV-U1-infected leaves at 48 hpi. *Bottom*: H_2O_2 level in TMV-U1 infected leaves at 72 hpi. For panels *B*, *D*, and *E*, error bars indicate mean ± SD (n = 4 biologically independent plants for panel *B*; n = 3 biologically independent plants for panels *D* and *E*). Asterisks indicated the significant difference based on two-sided paired Student's *t* test (*$P < 0.05$, **$P < 0.01$, ***$P < 0.001$). For panel *G*, error bars indicate mean ± SD (n = 4 biologically independent plants). Asterisks indicated the significant difference based on one-way ANOVA analysis with Dunnett's multiple comparison test (*$P < 0.05$, **$P < 0.01$, ***$P < 0.001$).

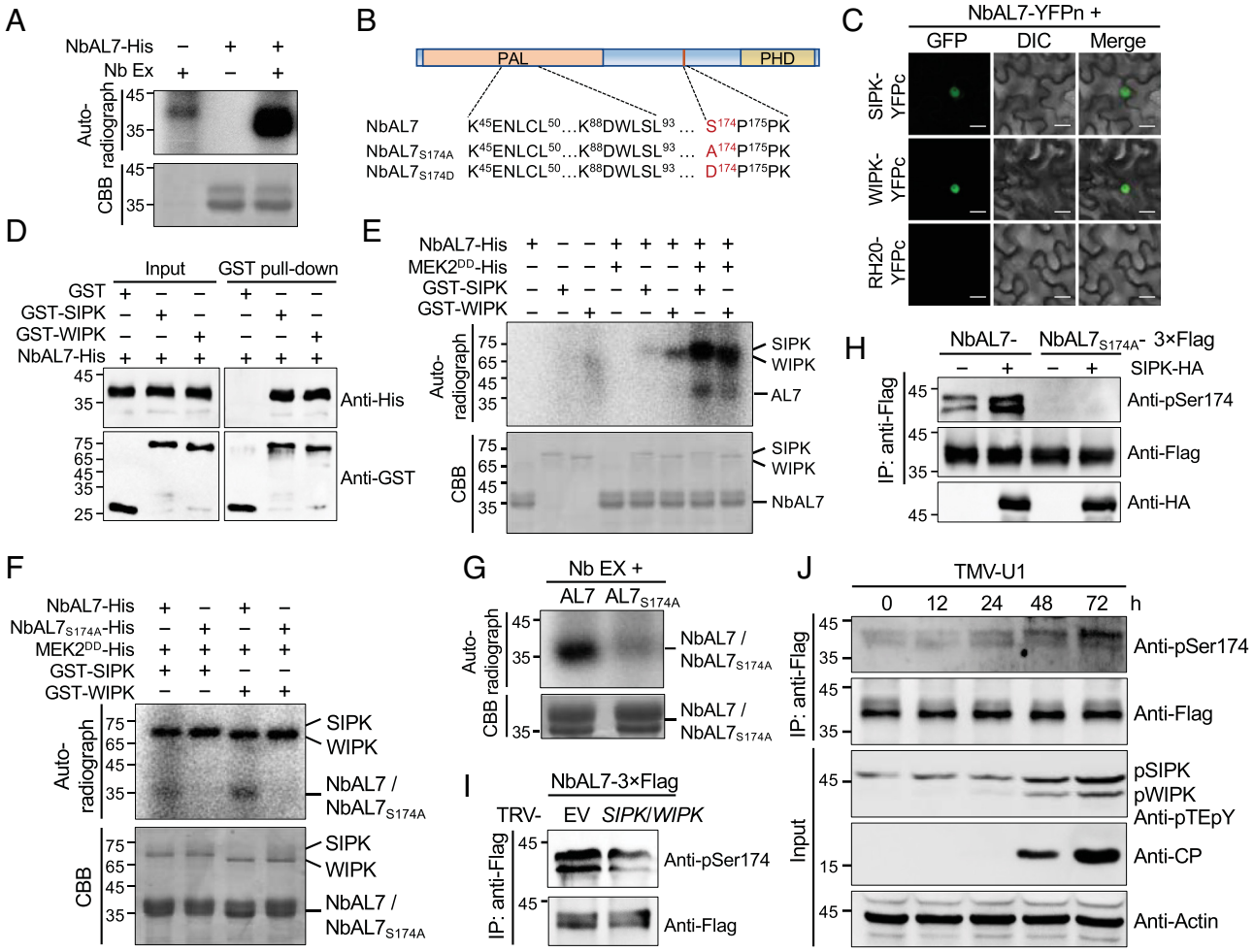

Fig. 5. SIPK/WIPK interact with and phosphorylate NbAL7 at Ser 174. (*A*) In vitro phosphorylation of His-tagged recombinant NbAL7 protein. The total soluble proteins extracted from healthy *N. benthamiana* leaves (Nb EX) were used as a kinase resource. Coomassie brilliant blue (CBB)-stained NbAL7-His are shown below. (*B*) Schematic representation of putative MAPK interaction motifs and phosphorylation site of NbAL7. $NbAL7_{S174A}$ and $NbAL7_{S174D}$ represent the phospho-null and phosphor-mimic mutants of NbAL7, respectively. (*C*) BiFC analysis of the interaction between NbAL7 and SIPK or WIPK. NbAL7-YFPn was coexpressed with SIPK-YFPc or WIPK-YFPc. RH20-YFPc served as a control. YFP signals were visualized by confocal microscopy at 48 hpi. (Scale bars, 15 μm.) (*D*) GST pull-down analysis of the interaction between NbAL7 and SIPK or WIPK. NbAL7-His or GFP-His was incubated with GST, GST-SIPK, or GST-WIPK. Input and pull-down products were analyzed by western blot with anti-His and anti-GST antibodies. (*E*) Phosphorylation of NbAL7 mediated by activated SIPK and WIPK in vitro. SIPK and WIPK were activated with recombinant $MEK2^{DD}$-His protein. Reactions lacking the specific components served as controls. Phosphorylated NbAL7 was detected by autoradiography after 12.5% sodium dodecyl sulphate polyacrylamide gel electrophoresis (SDS-PAGE) gel electrophoresis (*Upper*). CBB-stained SIPK, WIPK, and NbAL7 proteins were shown below. (*F*) Phosphorylation of NbAL7 and $NbAL7_{S174A}$ mediated by activated SIPK and WIPK in vitro. Recombinant NbAL7-His and $NbAL7_{S174A}$-His proteins were incubated with activated SIPK or WIPK. Phosphorylated NbAL7 or $NbAL7_{S174A}$ was detected by autoradiography after 12.5% SDS-PAGE gel electrophoresis (*Upper*). CBB-stained SIPK, WIPK, and AL7 are shown below. (*G*) In vitro phosphorylation assays of NbAL7 and $NbAL7_{S174A}$ by Nb EX. The autoradiography bands (*Upper*) and CBB-stained loading controls (*Bottom*) are shown. (*H*) SIPK-mediated phosphorylation of NbAL7 at Ser174 in vivo. *N. benthamiana* leaves transiently expressing NbAL7 or $NbAL7_{S174A}$ with or without SIPK were harvested at 48 hpi. Total proteins were immunoprecipitated with anti-Flag beads and detected by anti-Flag or anti-pSer174 polyclonal antibodies. SIPK expression was detected by Western blot with anti-HA antibody. (*I*) In vivo phosphorylation of NbAL7 at Ser174 in the tobacco rattle virus (TRV)-EV control and TRV-SIPK/WIPK inoculated *N. benthamiana*. NbAL7 and its derivatives were transiently expressed in upper silenced *N. benthamiana* leaves. At 2 dpi, total proteins were immunoprecipitated with anti-Flag beads and analyzed by western blot with anti-Flag or anti-pSer174 polyclonal antibodies. (*J*) TMV-induced NbAL7 phosphorylation at Ser174 depends on SIPK/WIPK. *NbAL7-OE* transgenic *N. benthamiana* leaves inoculated with 300 ng TMV-U1 virions were harvested at the indicated time points. Total proteins were immunoprecipitated with anti-Flag beads and detected by western blot with different polyclonal antibodies indicated on the right. Actin served as the loading control. For panels *C–E* and *H–J*, the experiments were independently repeated twice with similar results.

MAPKs (42). In addition, *N. benthamiana* WIPK and SIPK, the orthologs of *Arabidopsis* MPK3 and MPK6, were reported to be involved in *N*-mediated resistance pathway (19–21). Ser or Thr followed by Pro (SP or TP) is the minimal consensus motif for MAPK phosphorylation, and the docking domain which includes a cluster of basic residues upstream of the LxL motif ($[K/R]_{1-2}$ – x_{2-6} – [L/I] – x – [L/I]) were proved to be the MAPK kinases interacting motif (43). Interestingly, both SP/TP sites and docking domains were found in NbAL7 protein (Fig. 5*B*). These previous data implied that NbAL7 might be the substrate of SIPK and WIPK. To verify this, a BiFC assay was conducted to test their interactions. Coexpression of NbAL7-YFPn and SIPK/WIPK-YFPc in *N. benthamiana* leaves resulted in reconstitution of YFP signal in the nucleus compared to the control (Fig. 5*C*). The expression of target proteins in the BiFC assay was confirmed by immunoblot analysis (*SI Appendix*, Fig. S2*H*). Moreover, GST pull-down analysis revealed that NbAL7-His protein binds to either GST-SIPK or GST-WIPK, but not to GST control (Fig. 5*D*). These results indicate that SIPK and WIPK interact with NbAL7 in vivo and in vitro.

We next assessed whether NbAL7 is phosphorylated by SIPK and WIPK. Constitutively active $MEK2^{DD}$-activated GST-SIPK and GST-WIPK were able to phosphorylate NbAL7. By contrast, neither GST-SIPK nor GST-WIPK phosphorylated NbAL7-His

in the absence of constitutively active MEK2^{DD} (Fig. 5*E*). Two classical MAPK phosphorylation sites Ser174 and Thr228 followed by Pro were found in NbAL7, and Ser174 is highly conserved in AL7 from different plant species (*SI Appendix*, Fig. S7). Previous phosphoproteomic data from *A. thaliana* indicated the potential occurrence of phosphorylation at the Ser174 site (44). Thus, we mutated the Ser174 residue to Alanine within the NbAL7 protein and purified the recombinant NbAL7$_{S174A}$-His protein for in vitro phosphorylation assay. Interestingly, the phosphorylation signal produced by incubation of NbAL7$_{S174A}$-His with SIPK or WIPK was substantially reduced (Fig. 5*F*). Likewise, the phosphorylation signal for NbAL7$_{S174A}$ was also much lower than that of the NbAL7 in the presence of the *N. benthamiana* extracts (Fig. 5*G*). These results indicated that Ser174 is required for NbAL7 phosphorylation by SIPK/WIPK in vitro.

To determine the phosphorylation status of NbAL7 in vivo, we generated a polyclonal antibody that specifically recognizes the phosphorylated Ser174 in NbAL7. Given that transient expression of SIPK alone in tobacco leads to an increase of SIPK activity (19), we coexpressed SIPK with NbAL7 in *N. benthamiana* leaves and immunoblotting with anti-pSer174 showed an increased NbAL7 phosphorylation level at Ser174 site compared with expressing NbAL7 alone. No phosphorylation signal was detected for the NbAL7$_{S174A}$ mutant either in the absence or presence of SIPK (Fig. 5*H*). To further investigate whether the phosphorylation at Ser174 is mediated by SIPK/WIPK, TRV-based virus-induced gene silencing (VIGS) was used to downregulate the expression of both *SIPK* and *WIPK*. The NbAL7 was then transiently expressed in the upper uninoculated leaves where silencing occurs. Immunoblot with anti-pSer174 antibody revealed that the NbAL7 phosphorylation level was significantly reduced in plants where *SIPK* and *WIPK* expression was silenced (Fig. 5*I*). Moreover, we also constructed NbAL7 or NbAL7$_{S174A}$ fused to Flag tag under the control of its native promoter. *Agrobacterium* mixtures carrying the *ProNbAL7*::*NbAL7-3xFlag* or *ProNbAL7*::*NbAL7$_{S174A}$-3xFlag* and 35S::SIPK-HA were infiltrated into the *N. benthamiana* leaves. At 3 dpi, NbAL7-3xFlag protein was enriched by immunoprecipitation with anti-Flag beads; immunoblotting with anti-pSer174 showed consistent NbAL7 phosphorylation changes with that shown in Fig. 5 *H* and *I* (*SI Appendix*, Fig. S8). However, we observed no phosphorylation when expressed with the *NbAL7$_{S174A}$* mutant (*SI Appendix*, Fig. S8).

To test whether SIPK/WIPK-mediated phosphorylation of NbAL7 was induced during activation of *N*-mediated immune response, we inoculated TMV-U1 virions on *NbAL7-OE* plants, and the TMV-infected leaves were harvested at 0, 12, 24, 48, and 72 hpi. Immunoblot analysis revealed that the phosphorylation level of NbAL7 at Ser174 was increased during TMV infection (Fig. 5 *J*, *Upper*), which is in parallel with the activation of the MAPK cascade (Fig. 5 *J*, *Middle*). Together, these results indicated that NbAL7 is phosphorylated by SIPK/WIPK at the Ser174 site in vivo, a process induced by activation of *N*-mediated defense response.

SIPK/WIPK-Mediated NbAL7 Phosphorylation Promotes *N*-Mediated Immune Response. To investigate the influence of SIPK/WIPK-mediated phosphorylation on NbAL7 functions, we coexpressed SIPK with NbAL7 because overexpression of SIPK in plants was able to activate its kinase activity (19). The results showed that overexpression of SIPK in *N. benthamiana* induces mild cell death, which is consistent with the cell death triggered by overexpression of SIPK in *N. tabacum* (19). Intriguingly, trypan blue and DAB staining showed that coexpression of SIPK with NbAL7 induces more severe cell death phenotype and higher ROS accumulation than the leaves expressing either SIPK or NbAL7 alone (Fig. 6*A*). Consistently, NbAL7-induced ion leakage and H_2O_2 accumulation was increased by up to 64% and 73%, respectively, in the presence of SIPK (Fig. 6 *B* and *C*). Immunoblot analysis confirmed the expression of NbAL7-Flag and SIPK-HA in the infiltrated leaves (*SI Appendix*, Fig. S2*I*). We did not observe the apparent effect of WIPK overexpression on NbAL7-induced ROS accumulation and cell death (*SI Appendix*, Fig. S9), which can be partially explained by the inability to trigger cell death when WIPK is overexpressed in tobacco (19).

To further evaluate the influence of phosphorylation on the NbAL7 function, we compared the difference of ROS accumulation and cell death induced by NbAL7 and phospho-null NbAL7$_{S174A}$ or phospho-mimetic NbAL7$_{S174D}$. When expressing NbAL7 or its mutants alone, NbAL7$_{S174A}$ showed less ROS accumulation and weaker cell death than NbAL7, whereas NbAL7$_{S174D}$ induced more ROS accumulation and enhanced cell death than both NbAL7 and NbAL7$_{S174A}$ (Fig. 6*D*). Ion leakage measurement and H_2O_2 measurement further substantiated the NbAL7$_{S174D}$ phenotype (Fig. 6 *E* and *F*). Similar results were observed when coexpressing NbAL7 or its mutants with SIPK (*SI Appendix*, Fig. S10). Immunoblot analysis confirmed target protein expression in the infiltrated leaves (*SI Appendix*, Fig. S2*J*).

To further investigate the role of SIPK and WIPK in NbAL7-induced cell death, TRV-VIGS was used to downregulate SIPK and WIPK. We observed cell death in the unsilenced control leaves where NbAL7 was transiently overexpressed (Fig. 6*G*, TRV-EV). In contrast, cell death triggered by NbAL7 overexpression was significantly attenuated in leaves where *SIPK* and *WIPK* were simultaneously silenced (Fig. 6*G*, TRV-*SIPK*/*WIPK*). Furthermore, NbAL7-induced ion leakage in TRV-SIPK/WIPK plants was 48% lower than that in TRV-EV control plants (Fig. 6*H*). The downregulation of *SIPK* and *WIPK* was verified by RT-qPCR (Fig. 6*I*). These results indicated that SIPK/WIPK-mediated phosphorylation on Ser174 is necessary for NbAL7 to promote ROS accumulation and induce cell death.

We then performed in vitro phosphorylation-coupled EMSA to analyze the effects of SIPK/WIPK on NbAL7 binding to DNA in vitro. EMSA showed that the binding of the NbAL7 to *NbGPX2* promoter was significantly enhanced upon the addition of MEK2^{DD}-activated SIPK/WIPK compared with that treated with SIPK/WIPK alone (Fig. 6*J*). In contrast, the binding of recombinant maltose-binding protein (MBP)-NbAL7$_{S174A}$ to the *NbGPX2* promoter was significantly reduced compared with MBP-NbAL7 (Fig. 6*K*). Moreover, we used the dual-luciferase reporter system to determine the effect of SIPK on the NbAL7-mediated transcriptional regulation of the target genes. SIPK and NbAL7 under the control of 35S promoter were coexpressed with the luciferase driven by the promoters of *NbAPX2*, *NbGR*, or *NbGPX2*. The 35S promoter-controlled REN served as the internal control. The results showed that overexpression of NbAL7 inhibited the expression of its target genes, and introduction of SIPK further significantly reinforces the transcriptional suppression activity of NbAL7 (Fig. 6*L*). We also analyzed the transcriptional regulation activity of NbAL7$_{S174A}$ and NbAL7$_{S174D}$ mutants. The results showed that NbAL7$_{S174D}$ exhibited enhanced transcription suppression activity on target genes. In contrast, NbAL7$_{S174A}$ failed to repress the target gene transcription (Fig. 6*M*). The expressions of NbAL7 and its variants were confirmed by immunoblot analysis (*SI Appendix*, Fig. S2*K*). Together, these results indicate that SIPK/

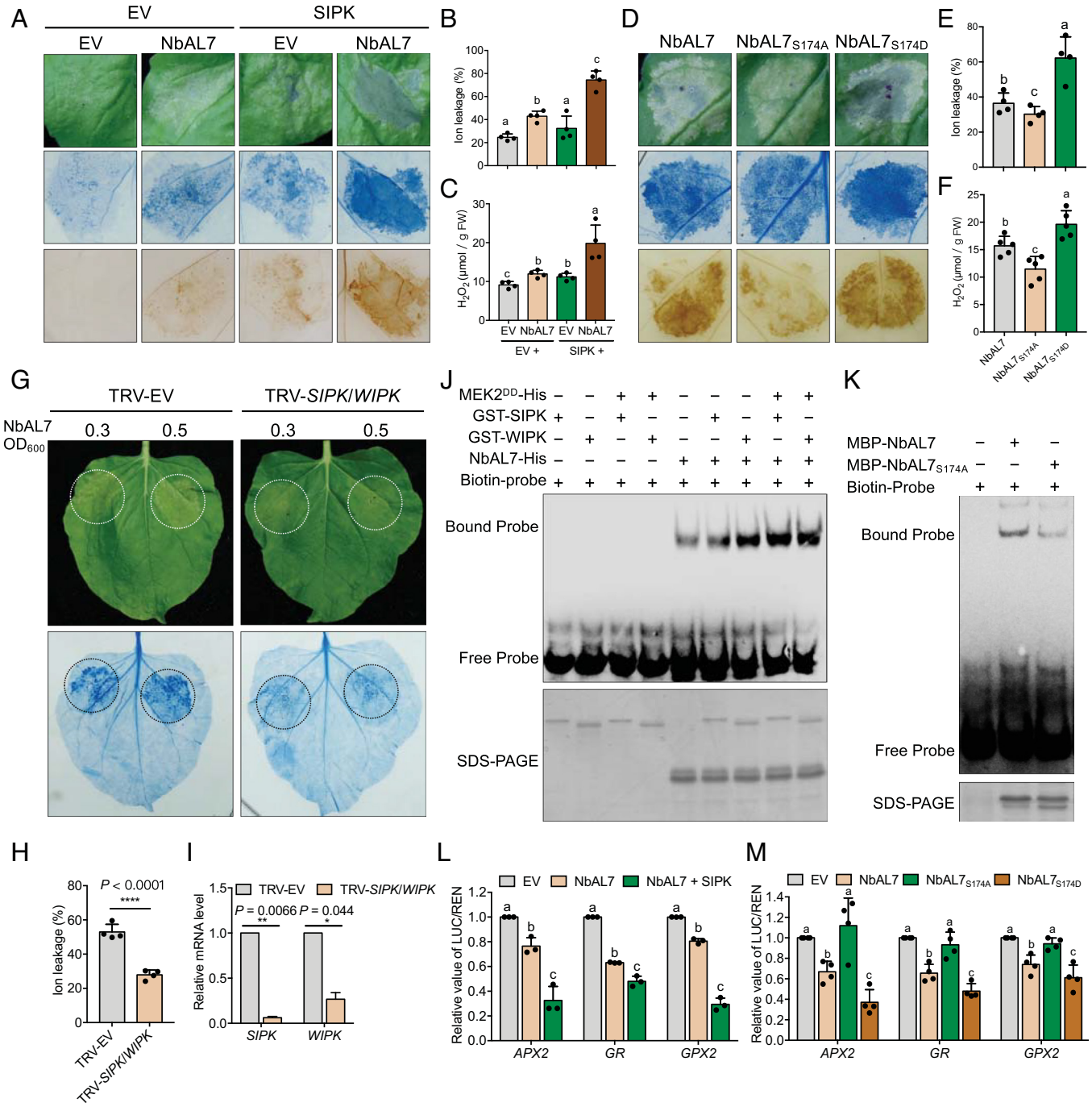

Fig. 6. SIPK/WIPK-mediated phosphorylation of NbAL7 enhances its transcriptional repressor activity. (*A*) NbAL7-induced ROS accumulation and cell death were enhanced by SIPK. *Agrobacterium* mixtures containing different plasmids as indicated above the panel were infiltrated into different regions of the same *N. benthamiana* leaves; leaf phenotypes (*Top*), trypan blue staining (*Middle*), and DAB staining (*Bottom*) are shown. Representative photographs were taken at 3 dpi. (*B* and *C*) Ion leakage assay (*B*) and measurement of H_2O_2 level (*C*) in the leaves shown in panel *A*. Error bars indicated mean ± SD (n = 4 biological independent plants). (*D*) Phosphorylation at Ser174 is required for NbAL7 to induce ROS accumulation and cell death. NbAL7, $NbAL7_{S174A}$, and $NbAL7_{S174D}$ were transiently expressed at different regions of the same *N. benthamiana* leaves. Leaf phenotypes (*Top*), trypan blue staining (*Middle*), and DAB staining (*Bottom*) are shown. Representative photographs were taken at 5 dpi. (*E* and *F*) Ion leakage assay (*E*) and measurement of the H_2O_2 level (*F*) in the leaves shown in panel *D*. Error bars indicate mean ± SD of the (n = 4 biological independent plants for panel *E* and n = 5 biological independent plants for panel *F*). (*G*) SIPK and WIPK were required for NbAL7-induced cell death. NbAL7 was transiently expressed in the upper silenced leaves of TRV-EV or TRV-*SIPK*/*WIPK*-inoculated *N. benthamiana*. Leaf phenotypes (*Top*) and trypan blue staining (*Bottom*) are shown. Representative photographs were taken at 3 dpi. (*H*) Quantification of cell death by measuring ion leakage of leaves shown in panel *G*. Error bars indicate ± SD of the mean (n = 4 biological independent plants). (*I*) RT-qPCR assay to confirm the downregulation of *SIPK* and *WIPK* mRNA. Error bars indicate ± SD of the mean (n = 2 independently replicates). Asterisks indicated the significant difference based on two-sided paired Student's *t* test (**P* < 0.05, ***P* < 0.01). (*J*) EMSA to test the effect of NbAL7 phosphorylation mediated by SIPK/WIPK on its DNA binding ability. After in vitro phosphorylation assays, a biotin-labeled *GPX2* DNA fragment was incubated with NbAL7-His or phosphorylated NbAL7-His protein. Bound probe and shift probe were detected with anti-Streptavidin-horse radish peroxidase (HRP) (*Upper*). CBB-stained SIPK, WIPK, and NbAL7 proteins are shown below. (*K*) Phosphorylation of NbAL7 at Ser174 site regulates its DNA binding ability. A biotin-labeled *GPX2* DNA fragment was incubated with MBP-NbAL7 or MBP-$NbAL7_{S174A}$ protein. Bound probe and shift probe were detected with anti-Streptavidin-HRP (*Upper*). CBB-stained MBP-NbAL7 and MBP-$NbAL7_{S174A}$ proteins are shown below. (*L*) NbAL7-mediated transcriptional suppression of *APX2, GR*, and *GPX2* was enhanced by SIPK. LUC activity was measured by normalizing to the REN signal. Error bars indicate mean ± SD (n = 3 biologically independent plants). (*M*) The effect of Ser174 phosphorylation on NbAL7 transcriptional repressor activity. LUC activity was measured by normalizing to the REN signal. Error bars indicate mean ± SD (n = 4 biologically independent plants). For panels *B* and *C*, *E* and *F*, and *L* and *M*, different letters in the chart indicate statistically significant differences among different groups according to the one-way ANOVA analysis with Dunnett's multiple comparison test (*P* < 0.05).

WIPK-mediated NbAL7 phosphorylation enhances its binding to the target genes, thus enabling suppression of ROS scavenging gene expression and promoting activation of *N*-mediated defense responses to TMV infection.

NbAL7 Phosphorylation Modulate Its Interaction with N Protein. Given the nucleocytoplasmic partitioning of N NLR receptor, we hypothesize that the interaction between N and TFs may be tightly regulated by immune activation. To test the dynamic interaction between NbAL7 and N protein during *N*-mediated defenses, NbAL7 and TIR domains of N were coexpressed in *NN* plants followed by Co-IP analysis, and p50 was introduced to activate *N*-mediated immunity. The results showed that less N-TIR was coimmunoprecipitated by NbAL7 in the presence of a p50 effector than that in the absence of p50 (*SI Appendix*, Fig. S11*A*). Likewise, the split luciferase assay showed that p50 expression significantly reduced the luminescence signal produced by the cLuc-NbAL7/TIR-nLuc in the leaves of *NN* plants (*SI Appendix*, Fig. S11*B*), suggesting that N-NbAL7 interaction was attenuated during *N*-mediated immune activation.

To investigate the effect of NbAL7 phosphorylation on its interaction with N, Co-IP was carried out to analyze the interaction between N and NbAL7 or its derivatives. Co-IP assays revealed that $NbAL7_{S174A}$ can be coimmunoprecipitated with N, which is comparable to that of the NbAL7. In contrast, the $NbAL7_{S174D}$ association with N was substantially reduced, similar to that of the negative citrine control (*SI Appendix*, Fig. S11*C*). We also performed split luciferase assay to further examine their interactions; the results showed that either cLuc-NbAL7 or cLuc-$NbAL7_{S174A}$ produced strong luminescence signals in the presence of TIR-nLuc. In contrast, we observed very weak luminescence signals in the region coexpressing cLuc-$NbAL7_{S174D}$ and TIR-nLuc (*SI Appendix*, Fig. S11*D*). Proteins in the split luciferase assays were successfully expressed as evidenced by immunoblot analysis (*SI Appendix*, Fig. S2 *L* and *M*). All these results demonstrate that phosphorylation at Ser174 of NbAL7 impairs the interaction between NbAL7 and N protein.

MAPK-AL7 Module Also Function in Other TNLs-Mediated Cell Death. The function of NbAL7 in suppressing ROS scavenging prompted us to investigate whether NbAL7 functions in other TNLs-mediated immunity besides the N TNL. We tested several TNL and effector combinations including HopQ1 and XopQ, which can be recognized by the *N. benthamiana* Roq1 TNL (45) and AvrRPS4 plus RRS1-R/RPS4 (46) in *NN*, *NbAL7-KO,* and *NbAL7-KD* plants, respectively. The results showed that cell death mediated by different TNLs was attenuated in the leaves of *NbAL7-KO* and *NbAL7-KD* plants compared with that of the *NN* plants (Fig. 7*A* and *SI Appendix*, Table S2), suggesting a broader role for the MAPK-AL7 module in different TNLs-mediated defense responses.

Discussion

Transcriptional reprogramming is a common event that occurs downstream of PTI and ETI. Although intensive studies have been performed to elucidate the role of diverse TFs in the plant defenses against bacteria and fungi, transcriptional reprogramming involved in NLR-mediated resistance against plant viruses remains largely underexplored. The N TNL is one of the well-studied viral NLRs that confers resistance against TMV (47). Here, we identified a plant homeodomain (PHD) domain-containing nuclear-localized NbAL7 protein as a new component of N NLR immune complexes by directly interacting with N protein. Our results demonstrated that NbAL7 acts as a transcriptional repressor that binds to the G-rich elements in the promoters of ROS scavenging genes and negatively regulates the expression of these genes, which leads to the ROS accumulation and rapid activation of *N*-mediated defense responses. We also show that the NbAL7 is directly phosphorylated and regulated by the MAPK cascade, thereby constituting a functional module to fine-tune the *N*-mediated immune response.

The AL PHD finger proteins have been reported to function in plant growth and development by regulating the histone modification status (48). In addition, AL family proteins also participate in plant tolerance to salt, cold, and drought stresses (27, 28). Very little is known about the function of AL family proteins during biotic stresses. Here, using *NbAL7* knock-down and knock-out plants, we demonstrated the importance of AL7 in *N*-mediated resistance against TMV, and the mechanisms underlying how NbAL7 contributes to *N*-mediated defense. Our study expands the current understanding of AL family proteins by demonstrating that they not only function in plant adaptation to abiotic stresses but also play an important role in plant response to biotic stresses, in particular NLR-mediated resistance against plant viruses.

We found that NbAL7 is a transcriptional repressor that positively regulates immunity, which is distinct from previously reported TFs that usually serve as transcriptional activators to promote the expression of defense-related genes like *PR1*, *EDS1*, and *ADR1* (49, 50). Our ChIP-seq analysis and further molecular analysis showed that NbAL7 directly targets a set of ROS scavenging genes, indicating that NbAL7 functions to promote ROS accumulation to induce defense (Fig. 7*B*). Interestingly, N interaction with NbAL7 was attenuated in the presence of TMV p50 effector indicating that the free NbAL7 could bind to and repress ROS scavenging genes to promote ROS accumulation and induction of defense (Fig. 7*B*). In contrast to NbAL7, previously we have shown that SPL6 TF associates with N only in the presence of p50 effector to positively modulate *N*-mediated defense (23). These findings indicate that N TNL interacts with different TFs with activation and repressor functions to orchestrate immunity.

ROS is an important signaling component not only in immunity but also in maintaining normal plant growth and development (39, 51, 52). However, overproduction of ROS is harmful to plant growth and development. Therefore, under normal conditions, the ROS level is tightly controlled by multiple regulatory systems for redox homeostasis (36, 53). However, upon pathogen attack, this homeostasis is disrupted, leading to the ROS accumulation in different cell compartments and activation of the immune system to cope with the infection of pathogen. This can be accomplished either by upregulating the expression of ROS-producing enzymes (e.g., respiratory burst oxidase homolog D) or by turning off the ROS scavenging system. Although a number of TFs like WRKY7/8/9/11, NTL4, TaSNAC11-4B, and bHLH123 have been reported to directly enhance ROS production by increasing the transcription of ROS production-related genes (54–57), how ROS scavenging-associated genes expression is regulated during plant defense remains largely unknown. Our findings revealed that NbAL7 acts as a hitherto uncharacterized transcriptional repressor that directly inhibits the transcription of ROS scavenging enzymes like APX2, GR, and GPX2 during *N*-mediated resistance against TMV. These results further enriched the transcriptional regulatory network underlying ROS production and provide evidence that different TFs concertedly regulate ROS production and scavenging to achieve rapid accumulation of ROS during immunity.

Some of the TFs involved in plant immunity are known to be subjected to posttranslational modifications (58–60). Among them, phosphorylation of TFs during plant immune signaling is one of the frequently observed events, and calcium-dependent protein kinases (CDPKs) and MAPKs are two of the largest

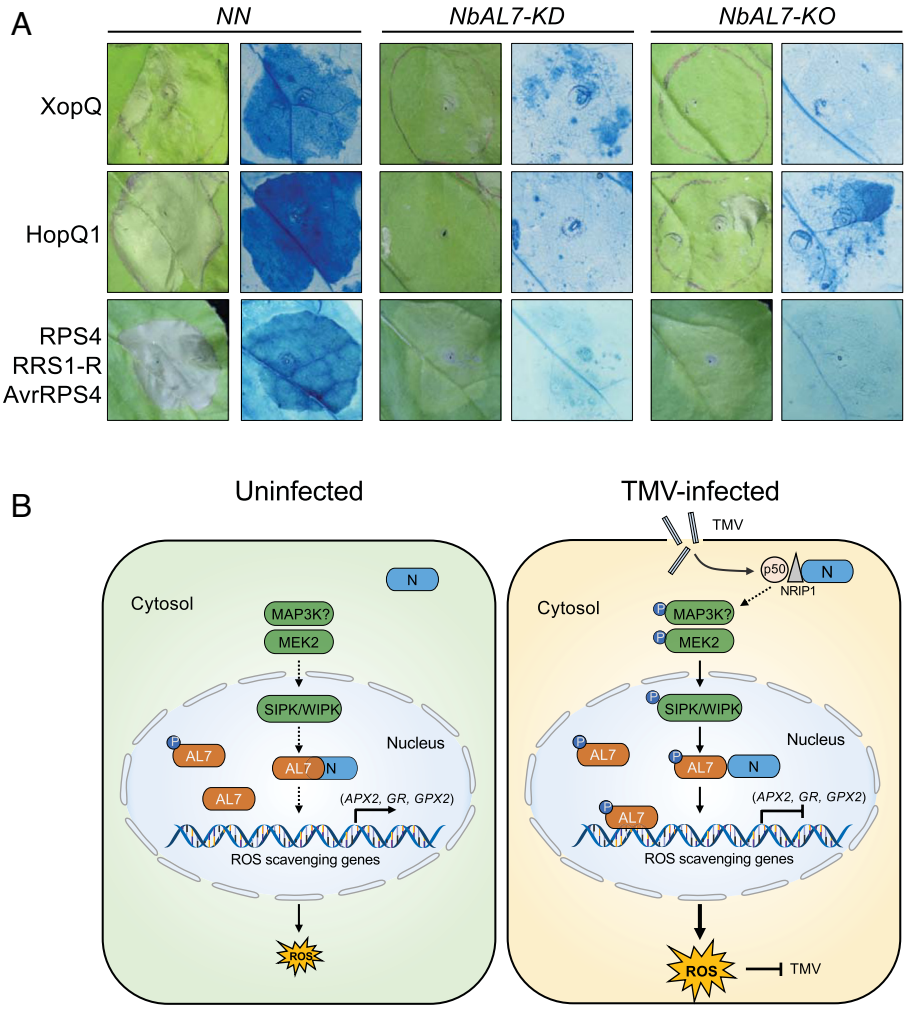

Fig. 7. Roles of NbAL7 in other TNLs-mediated immunity. (*A*) Phenotypes of leaves expressing different effector or effect/NLR proteins. Leaves of *NN, NbAL7-KO*, and *NbAL7-KD N. benthamiana* plants were infiltrated with *Agrobacterium* mixtures harboring plasmids expressing different proteins as indicated on the left. The infiltrated plants were transferred to the laboratory 24 h after infiltration. Leaves were stained by trypan blue and representative photographs were taken at 3.5 dpi. (*B*) A proposed model for illustrating the functional role of MAPK-NbAL7 module in *N*-mediated resistance against TMV. Under normal conditions, NbAL7 proteins with low levels of Ser174 phosphorylation interacts with N protein and showed relatively weak DNA binding affinity and transcriptional repression activity, resulting in the expression of ROS scavenging genes, which is conducive to maintaining basal cellular level of ROS. Upon perception of TMV infection, the MAPK cascade was activated. The SIPK/WIPK interact and phosphorylate NbAL7, which impairs its interaction with N and enhances its binding to the promoters of ROS scavenging genes. The transcription of *APX2, GR*, and *GPX2* were then inhibited, which will promote ROS accumulation and elicit resistance against TMV infection.

families reported to be involved in this process (61). Here, we show that NbAL7 is a new substrate of SIPK and WIPK, and in vitro and in vivo biochemical assays showed that Ser174 of NbAL7 is phosphorylated by these MAPKs (Fig. 5 *F–I*). Even after several attempts, we failed to identify the Ser174 phosphorylation by the liquid chromatography-tandem mass spectrometry (LC-MS/MS) method (*SI Appendix*, Fig. S12). We reason that the Ser174 phosphorylation affects the trypsin digestion on K172 and K177, or digestion at these two sites produced short peptides that were hard to be enriched by the column (*SI Appendix*, Fig. S7). Since Ser174 is highly conserved in AL7s from diverse plant species (*SI Appendix*, Fig. S7), MAPK-AL7 constitutes an important signaling module in ETI.

Several studies have revealed that MAPK-mediated phosphorylation regulates different properties of TFs. For example, MPK3/MPK6-mediated phosphorylation of WRKY33 enhances its transactivation activity of WRKY33, leading to the enhanced expression of camalexin biosynthetic genes (9, 62). MPK4-mediated phosphorylation of ASR3 enhances its DNA binding ability, resulting in the suppression of plant immunity (63). In addition, phosphorylation of TFs by MAPKs also affects their interaction with other proteins. For instance, PBI1 interacts with transcriptional activator WRKY45 to negatively regulate its activity, whereas MPK3/MPK6 phosphorylated WRKY45 to release the inhibition of PBI1 on WRKY45 activity (64). Here, we show that phosphorylation of NbAL7 by SIPK/WIPK enhances its DNA binding ability and impairs the interaction between NbAL7 and N TNL. Our results, together with previous studies, collectively suggested that MAPK-mediated phosphorylation of downstream TFs for transcriptional reprogramming is a highly conserved event during *NLR*-mediated defense responses. Consistent with this, NbAL7 also positively regulates Roq1- and RPS4-mediated cell death.

Based on our findings described in this paper, we propose a model for the MAPK-AL7 functional module in NLR-mediated defense response. Under normal conditions, NbAL7 with a lower phosphorylation level interacts strongly with the N protein and has relatively low DNA binding ability, so the transcription of ROS scavenging genes like *APX2*, *GR*, and *GPX2* is less affected and can proceed normally, which is conducive to maintaining the basal levels of ROS that is critical for normal cellular function. Upon perception of TMV by N, MAPK cascades are activated and the SIPK/WIPK phosphorylate NbAL7, which leads to the release of NbAL7 from N NLR immune receptor complex and enhances its ability to bind to the promoters of ROS scavenging genes. The transcriptions of *APX2*, *GR*, and *GPX2* were then inhibited, creating an environment favorable for ROS accumulation and thereby eliciting resistance against TMV infection (Fig. 7*B*). Our results reveal a hitherto uncharacterized role for AL proteins in regulating plant innate immunity, which expands current understanding of the immune signaling network underlying *NLR*-mediated defense response.

Materials and Methods

Details of the materials and methods used in this paper, including plasmid constructions, generation of transgenic *N. benthamiana* plants and plant growth conditions, BiFC and split-luciferase assay, Co-IP, GST, or MBP pull-down assay, nuclei isolation from leaves, cell death induction, Trypan blue and DAB staining, ion leakage and H_2O_2 measurement, transaction activity assay in yeast, dual luciferase reporter system, EMSA, ChIP-seq, and ChIP-qPCR, in vitro and in vivo phosphorylation assay, and quantification and statistical analysis, are provided in *SI Appendix, Supporting Information Text: Materials and Methods*.

Data, Materials, and Software Availability. The data reported in this paper have been deposited in the National Center for Biotechnology Information Sequence Read Archive (BioProject accession no. PRJNA865533) (65).

ACKNOWLEDGMENTS. We would like to thank Dr. Nan Ma (China Agricultural University) for providing dual-luciferase reporter system-related vectors, Dr. Bo Li (Huazhong Agricultural University) for suggestions on the ChIP-Seq analysis, and Dr. Zhen Li (China Agricultural University) for technical assistance with LC-MS/MS analysis. We also thank Drs. Jialin Yu, Xian-Bing Wang, Chenggui Han, and Dongtao Ren at China Agricultural University for their valuable suggestions. This work was supported by grants from the National Natural Science Foundation of China (32122070 and 31872637). The NLR work in the SPD-K lab was supported by National Science Foundation (NSF) (IOS-1354434 and IOS-1339185).

Author affiliations: [a]State Key Laboratory of Plant Environmental Resilience and Ministry of Agriculture Key Laboratory of Soil Microbiology, College of Biological Sciences, China Agricultural University, Beijing 100193, China; [b]State Key Laboratory of Agro-Biotechnology and Ministry of Agriculture Key Laboratory of Pest Monitoring and Green Management, College of Plant Protection, China Agricultural University, Beijing 100193, China; and [c]Department of Plant Biology and the Genome Center, College of Biological Sciences, University of California, Davis, CA 95616

1. J. D. Jones, J. L. Dangl, The plant immune system. *Nature* **444**, 323–329 (2006).
2. C. G. Lee, C. A. Da Silva, J.-Y. Lee, D. Hartl, J. A. Elias, Chitin regulation of immune responses: An old molecule with new roles. *Curr. Opin. Immunol.* **20**, 684–689 (2008).
3. D. Chinchilla, Z. Bauer, M. Regenass, T. Boller, G. Felix, The *Arabidopsis* receptor kinase FLS2 binds flg22 and determines the specificity of flagellin perception. *Plant Cell* **18**, 465–476 (2006).
4. H. Cui, K. Tsuda, J. E. Parker, Effector-triggered immunity: From pathogen perception to robust defense. *Annu. Rev. Plant Biol.* **66**, 487–511 (2015).
5. B. P. M. Ngou, H. K. Ahn, P. Ding, J. D. G. Jones, Mutual potentiation of plant immunity by cell-surface and intracellular receptors. *Nature* **592**, 110–115 (2021).
6. M. Yuan *et al.*, Pattern-recognition receptors are required for NLR-mediated plant immunity. *Nature* **592**, 105–109 (2021).
7. M. Yuan, B. P. M. Ngou, P. Ding, X. F. Xin, PTI-ETI crosstalk: An integrative view of plant immunity. *Curr. Opin. Plant Biol.* **62**, 102030 (2021).
8. M. Chang, H. Chen, F. Liu, Z. Q. Fu, PTI and ETI: Convergent pathways with diverse elicitors. *Trends Plant Sci.* **27**, 113–115 (2022).
9. X. Meng, S. Zhang, MAPK cascades in plant disease resistance signaling. *Annu. Rev. Phytopathol.* **51**, 245–266 (2013).
10. J. Caplan, M. Padmanabhan, S. P. Dinesh-Kumar, Plant NB-LRR immune receptors: From recognition to transcriptional reprogramming. *Cell Host Microbe* **3**, 126–135 (2008).
11. C. Chang *et al.*, Barley MLA immune receptors directly interfere with antagonistically acting transcription factors to initiate disease resistance signaling. *Plant Cell* **25**, 1158–1173 (2013).
12. K. Zhai *et al.*, RRM transcription factors interact with NLRs and regulate broad-spectrum blast resistance in rice. *Mol. Cell* **74**, 996–1009.e7 (2019).
13. J. Chakraborty, P. Priya, S. G. Dastidar, S. Das, Physical interaction between nuclear accumulated CC-NB-ARC-LRR protein and WRKY64 promotes EDS1 dependent *Fusarium wilt* resistance in chickpea. *Plant Sci.* **276**, 111–133 (2018).
14. J. Kourelis, R. A. L. van der Hoorn, Defended to the nines: 25 years of resistance gene cloning identifies nine mechanisms for R protein function. *Plant Cell* **30**, 285–299 (2018).
15. S. Whitham *et al.*, The product of the tobacco mosaic virus resistance gene *N*: Similarity to toll and the interleukin-1 receptor. *Cell* **78**, 1101–1115 (1994).
16. J. L. Caplan, P. Mamillapalli, T. M. Burch-Smith, K. Czymmek, S. P. Dinesh-Kumar, Chloroplastic protein NRIP1 mediates innate immune receptor recognition of a viral effector. *Cell* **132**, 449–462 (2008).
17. F. L. Erickson *et al.*, The helicase domain of the TMV replicase proteins induces the *N*-mediated defence response in tobacco. *Plant J.* **18**, 67–75 (1999).
18. P. Mestre, D. C. Baulcombe, Elicitor-mediated oligomerization of the tobacco N disease resistance protein. *Plant Cell* **18**, 491–501 (2006).
19. S. Zhang, Y. Liu, Activation of salicylic acid-induced protein kinase, a mitogen-activated protein kinase, induces multiple defense responses in tobacco. *Plant Cell* **13**, 1877–1889 (2001).
20. Y. Liu *et al.*, Interaction between two mitogen-activated protein kinases during tobacco defense signaling. *Plant J.* **34**, 149–160 (2003).
21. S. Zhang, D. F. Klessig, Resistance gene *N*-mediated *de novo* synthesis and activation of a tobacco mitogen-activated protein kinase by tobacco mosaic virus infection. *Proc. Natl. Acad. Sci. U.S.A.* **95**, 7433–7438 (1998).
22. R. Hoser *et al.*, Nucleocytoplasmic partitioning of tobacco N receptor is modulated by SGT1. *New Phytol.* **200**, 158–171 (2013).
23. M. S. Padmanabhan *et al.*, Novel positive regulatory role for the SPL6 transcription factor in the N TIR-NB-LRR receptor-mediated plant innate immunity. *PLoS Pathog.* **9**, e1003235 (2013).
24. Y. Zhang *et al.*, TurboID-based proximity labeling reveals that UBR7 is a regulator of N NLR immune receptor-mediated immunity. *Nat. Commun.* **10**, 3252 (2019).
25. W. Y. Lee, D. Lee, W. I. Chung, C. S. Kwon, Arabidopsis ING and Alfin1-like protein families localize to the nucleus and bind to H3K4me3/2 via plant homeodomain fingers. *Plant J.* **58**, 511–524 (2009).
26. A. M. Molitor, Z. Bu, Y. Yu, W. H. Shen, *Arabidopsis* AL PHD-PRC1 complexes promote seed germination through H3K4me3-to-H3K27me3 chromatin state switch in repression of seed developmental genes. *PLoS Genet.* **10**, e1004091 (2014).
27. W. Wei *et al.*, The Alfin-like homeodomain finger protein AL5 suppresses multiple negative factors to confer abiotic stress tolerance in Arabidopsis. *Plant J.* **81**, 871–883 (2015).
28. J. J. Tao *et al.*, An *Alfin-like* gene from *Atriplex hortensis* enhances salt and drought tolerance and abscisic acid response in transgenic Arabidopsis. *Sci. Rep.* **8**, 2707 (2018).
29. H. Chen *et al.*, Firefly luciferase complementation imaging assay for protein-protein interactions in plants. *Plant Physiol.* **146**, 323–324 (2007).
30. Y. Liu, M. Schiff, R. Marathe, S. P. Dinesh-Kumar, Tobacco *Rar1*, *EDS1* and *NPR1/NIM1* like genes are required for *N*-mediated resistance to tobacco mosaic virus. *Plant J.* **30**, 415–429 (2002).
31. Y. Liu *et al.*, MYC2 regulates the termination of jasmonate signaling via an autoregulatory negative feedback loop. *Plant Cell* **31**, 106–127 (2019).
32. R. Mittler, E. Lam, V. Shulaev, M. Cohen, Signals controlling the expression of cytosolic ascorbate peroxidase during pathogen-induced programmed cell death in tobacco. *Plant Mol. Biol.* **39**, 1025–1035 (1999).
33. R. Mittler, S. Vanderauwera, M. Gollery, F. Van Breusegem, Reactive oxygen gene network of plants. *Trends Plant Sci.* **9**, 490–498 (2004).
34. K. Asada, Production and scavenging of reactive oxygen species in chloroplasts and their functions. *Plant Physiol.* **141**, 391–396 (2006).
35. M. A. Inupakutika, S. Sengupta, A. R. Devireddy, R. K. Azad, R. Mittler, The evolution of reactive oxygen species metabolism. *J. Exp. Bot.* **67**, 5933–5943 (2016).
36. M. Gao *et al.*, Ca^{2+} sensor-mediated ROS scavenging suppresses rice immunity and is exploited by a fungal effector. *Cell* **184**, 5391–5404.e5317 (2021).
37. P. Liu *et al.*, A virus-derived siRNA activates plant immunity by interfering with ROS scavenging. *Mol. Plant* **14**, 1088–1103 (2021).
38. B. Chandrasekar *et al.*, Fungi hijack a ubiquitous plant apoplastic endoglucanase to release a ROS scavenging β-glucan decasaccharide to subvert immune responses. *Plant Cell* **34**, 2765–2784 (2022).
39. J. Qi, J. Wang, Z. Gong, J. M. Zhou, Apoplastic ROS signaling in plant immunity. *Curr. Opin. Plant Biol.* **38**, 92–100 (2017).
40. N. Doke, Y. Ohashi, Involvement of an O_2^- generating system in the induction of necrotic lesions on tobacco leaves infected with tobacco mosaic virus. *Physiol. Mol. Plant Pathol.* **32**, 163–175 (1988).
41. L. Kiraly, Y. M. Hafez, J. Fodor, Z. Kiraly, Suppression of tobacco mosaic virus-induced hypersensitive-type necrotization in tobacco at high temperature is associated with downregulation of NADPH oxidase and superoxide and stimulation of dehydroascorbate reductase. *J. Gen. Virol.* **89**, 799–808 (2008).
42. S. C. Popescu *et al.*, MAPK target networks in *Arabidopsis thaliana* revealed using functional protein microarrays. *Genes Dev.* **23**, 80–92 (2009).
43. A. D. Sharrocks, S. H. Yang, A. Galanis, Docking domains and substrate-specificity determination for MAP kinases. *Trends Biochem. Sci.* **25**, 448–453 (2000).
44. S. Reiland *et al.*, Large-scale Arabidopsis phosphoproteome profiling reveals novel chloroplast kinase substrates and phosphorylation networks. *Plant Physiol.* **150**, 889–903 (2009).
45. A. Schultink, T. Qi, A. Lee, A. D. Steinbrenner, B. Staskawicz, Roq1 mediates recognition of the Xanthomonas and Pseudomonas effector proteins XopQ and HopQ1. *Plant J.* **92**, 787–795 (2017).
46. P. F. Sarris *et al.*, A plant immune receptor detects pathogen effectors that target WRKY transcription factors. *Cell* **161**, 1089–1100 (2015).
47. P. Kapos, K. T. Devendrakumar, X. Li, Plant NLRs: From discovery to application. *Plant Sci.* **279**, 3–18 (2019).
48. M. A. Kayum *et al.*, Characterization and stress-induced expression analysis of Alfin-like transcription factors in *Brassica rapa*. *Mol. Genet. Genomics* **290**, 1299–1311 (2015).
49. J. Choi *et al.*, The cytokinin-activated transcription factor ARR2 promotes plant immunity via TGA3/NPR1-dependent salicylic acid signaling in Arabidopsis. *Dev. Cell* **19**, 284–295 (2010).
50. T. Sun *et al.*, ChIP-seq reveals broad roles of SARD1 and CBP60g in regulating plant immunity. *Nat. Commun.* **6**, 10159 (2015).
51. A. Baxter, R. Mittler, N. Suzuki, ROS as key players in plant stress signalling. *J. Exp. Bot.* **65**, 1229–1240 (2014).
52. D. Camejo, A. Guzman-Cedeno, A. Moreno, Reactive oxygen species, essential molecules, during plant-pathogen interactions. *Plant Physiol. Biochem.* **103**, 10–23 (2016).
53. C. Waszczak, M. Carmody, J. Kangasjarvi, Reactive oxygen species in plant signaling. *Annu. Rev. Plant Biol.* **69**, 209–236 (2018).
54. S. Lee, P. J. Seo, H. J. Lee, C. M. Park, A NAC transcription factor NTL4 promotes reactive oxygen species production during drought-induced leaf senescence in *Arabidopsis*. *Plant J.* **70**, 831–844 (2012).
55. H. Adachi *et al.*, WRKY transcription factors phosphorylated by MAPK regulate a plant immune NADPH oxidase in *Nicotiana benthamiana*. *Plant Cell* **27**, 2645–2663 (2015).
56. Z. Zhang, C. Liu, Y. Guo, Wheat transcription factor TaSNAC11-4B positively regulates leaf senescence through promoting ROS production in transgenic *Arabidopsis*. *Int. J. Mol. Sci.* **21**, 7672 (2020).
57. W. B. Zhang *et al.*, Arabidopsis NF-YCs play dual roles in repressing brassinosteroid biosynthesis and signaling during light-regulated hypocotyl elongation. *Plant Cell* **33**, 2360–2374 (2021).
58. H. A. van den Burg, F. L. Takken, SUMO-, MAPK-, and resistance protein-signaling converge at transcription complexes that regulate plant innate immunity. *Plant Signal Behav.* **5**, 1597–1601 (2010).
59. J. Withers, X. Dong, Post-translational regulation of plant immunity. *Curr. Opin. Plant Biol.* **38**, 124–132 (2017).
60. D.W.-K. Ng, J. K. Abeysinghe, M. Kamali, Regulating the regulators: The control of transcription factors in plant defense signaling. *Int. J. Mol. Sci.* **19**, 3737 (2018).
61. M. Boudsocq, J. Sheen, CDPKs in immune and stress signaling. *Trends Plant Sci.* **18**, 30–40 (2013).
62. J. Zhou *et al.*, Differential phosphorylation of the transcription factor WRKY33 by the protein kinases CPK5/CPK6 and MPK3/MPK6 cooperatively regulates aamalexin biosynthesis in Arabidopsis. *Plant Cell* **32**, 2621–2638 (2020).
63. B. Li *et al.*, Phosphorylation of trihelix transcriptional repressor ASR3 by MAP KINASE4 negatively regulates *Arabidopsis* immunity. *Plant Cell* **27**, 839–856 (2015).
64. K. Ichimaru *et al.*, Cooperative regulation of PBI1 and MAPKs controls WRKY45 transcription factor in rice immunity. *Nat. Commun.* **13**, 2397 (2022).
65. D. Zhang, ChIP-seq and Genome-wide identification of AL7 targets in *Nicotiana benthamiana*. *SRA Database*. https://www.ncbi.nlm.nih.gov/bioproject/PRJNA865533. Deposited 3 August 2022.